Intrinsic methane steam reforming kinetics on nickel-ceria solid oxide fuel cell anodes

van Biert, Lindert; Visser, K.; Aravind, P. V.

DOI
10.1016/j.jpowsour.2019.227261

Publication date
2019

Document Version
Final published version

Published in
Journal of Power Sources

Journal of Power Sources 443 (2019) 227261

Contents lists available at ScienceDirect

Journal of Power Sources

journal homepage: www.elsevier.com/locate/jpowsour

Intrinsic methane steam reforming kinetics on nickel-ceria solid oxide fuel cell anodes

L. van Biert [a,b,*], K. Visser [a], P.V. Aravind [b]

[a] Department of Maritime & Transport Technology, Delft University of Technology, Mekelweg 2, 2628 CD, Delft, the Netherlands
[b] Department of Process & Energy, Delft University of Technology, Leeghwaterstraat 39, 2628 CB, Delft, the Netherlands

HIGHLIGHTS

- Methane steam reforming is experimentally studied on nickel-ceria anodes.
- The methane, steam and hydrogen partial pressures are varied in the experiment. .
- Several kinetic models are parameterised with the experimental data and compared.
- A Langmuir-Hinshelwood reaction mechanism is found to be most adequate.

ABSTRACT

Direct internal reforming in solid oxide fuel cells (SOFCs) is advantageous as it enables to heat and steam from the exothermic hydrogen oxidation reaction in the endothermic steam reforming reaction. However, it may increase potentially deteriorating temperature gradients as well. The temperature and concentration profiles can be accurately simulated with adequate SOFC models and intrinsic methane steam reforming (MSR) kinetics. Therefore, this study aims to derive intrinsic MSR kinetics suitable for control-oriented dynamic SOFC models. The individual influences of the methane, steam and hydrogen partial pressures on the MSR reaction are experimentally studied on functional electrolyte supported cells with nickel-gadolinium doped cerium anodes. A non-proportional dependence of the MSR rate on the methane partial pressure and a slight negative dependence on the steam partial pressure are observed, but the effect of the hydrogen partial pressure seems insignificant. Various kinetic rate equations are parameterised with the experimental data and an ideal plug flow reactor model. An intrinsic Langmuir-Hinshelwood mechanism for a rate determining step between associatively adsorbed methane and dissociatively adsorbed steam on the catalyst surface shows good agreement with the experimental data, and is thermodynamically and physically consistent.

1. Introduction

Global agreements to eliminate greenhouse gas and hazardous air pollutant emissions from human activities drive the need for intrinsically clean energy conversion technologies [1,2]. Electrochemical conversion of renewable electricity to synthetic fuels through electrolysis may play a key role in storage and distribution of energy in future energy systems, as these can be easily transported and stored [3]. In addition, fuel cells enable efficient electrochemical conversion of these renewable fuels to electricity emitting virtually no hazardous air pollutants [4]. Therefore, these technologies can facilitate an infrastructure for renewable energy which is entirely free of hazardous emissions.

Hydrogen is a well-known potential renewable energy carrier, but has a relatively low volumetric energy density compared to liquid fuels. Therefore, energy carriers with a higher volumetric energy density may be required for long distance mobility, such as aerospace or intercontinental maritime transport [5]. For example, methanol or methane synthesised from renewable sources can be stored with energy densities similar to liquefied natural gas, which is readily adopted in the maritime industry as a low-carbon transition fuel.

Energy dense hydrocarbon fuels are usually converted to a hydrogen rich gas before they can be electrochemically oxidised. While low temperature fuel cells require external processing of hydrocarbon fuels to a relatively pure hydrogen flow, solid oxide fuel cells (SOFCs) enable direct internal reforming (DIR) of light hydrocarbons, such as methane [6]. DIR on the SOFC anode enables the use of heat and steam produced by the electrochemical reaction to reform methane. Therefore, DIR is more efficient than external reforming. Moreover, the amount of excess air that has to be supplied to control the temperature of the stack is reduced by the cooling endothermic reforming reaction, subsequently lowering the auxiliary power consumed by the air blower [7].

The endothermic reforming reaction is reported to occur primarily at

* Corresponding author. Department of Maritime & Transport Technology, Delft University of Technology, Mekelweg 2, 2628 CD, Delft, the Netherlands.
E-mail address: l.vanbiert@tudelft.nl (L. van Biert).

https://doi.org/10.1016/j.jpowsour.2019.227261
Received 14 July 2019; Received in revised form 5 September 2019; Accepted 2 October 2019
Available online 9 October 2019

the inlet section of the stack, where the methane concentration is highest. In contrast, the exothermic hydrogen oxidation reaction rate typically increases towards the outlet, where the temperature and subsequently the ionic conductivity of the electrolyte is higher [8]. As a result, DIR may induce steep concentration and temperature gradients within the SOFC stack, which may compromise the electrochemical performance and induce deteriorating thermal stresses [9].

The severity of the thermal stresses caused by DIR depends on the amount of hydrocarbons in the fuel gas and the reforming reaction rate on the SOFC anode [10]. Therefore, safe and reliable operation of SOFCs fuelled with hydrocarbons requires detailed understanding of the kinetics of the reforming reaction, and how these are affected by stack operating conditions, such as temperature, steam-to-carbon ratio and the amount of pre-reforming employed before the fuel enters the anode compartment [11].

The kinetics of the methane reforming reaction have been subject of many studies, both for industrial steam reformers and SOFCs, because:

- Methane is a simple and abundant hydrocarbon molecule;
- Methane is the main constituent of natural gas [12,13];
- (Pre)-reforming of other hydrocarbons and alcohols, such as methanol, yields methane [14,15].

Methane is most commonly converted to a hydrogen rich mixture through the methane steam reforming (MSR) and water gas shift (WGS) reactions,

$$CH_4 + H_2O \rightleftharpoons 3H_2 + CO \quad (1)$$

$$CO + H_2O \rightleftharpoons H_2 + CO_2 \quad (2)$$

respectively, after which the hydrogen produced can be subsequently oxidised in the fuel cell to produce electricity:

$$H_2 + \frac{1}{2}O_2 \Rightarrow H_2O \quad (3)$$

The MSR reaction has been studied extensively for commercial steam reformers to produce hydrogen from natural gas. More recently, researchers have investigated the kinetics of the steam reforming reaction on SOFC anode materials as well. Three classes of MSR kinetics may be distinguished in these studies: Multi-step reaction mechanisms, surface reaction models assuming a rate determining step on a catalyst, and empirical global power law (PL) kinetics. Comprehensive overviews of methane steam reforming in SOFCs have been presented in dedicated literature reviews [16,17].

Multi-step mechanisms describe the kinetics with a sequence of intermediate steps, consisting of adsorption, surface reaction and desorption processes. The rate is determined by the slowest intermediate reaction or co-limited by several slow steps, which may change for different temperature as well as reactant and product partial pressures. A heterogeneous multi-step mechanism consisting of 42 different intermediate reactions was derived by Hecht et al. [18] for a nickel-yttrium stabilised zirconia (Ni-YSZ) cermet anode.

In classical surface chemistry theory, the overall reaction kinetics are described by a single rate determining step [19]. Langmuir-Hinshelwood (LH), Hougen-Watson (HW) and Eley-Rideal kinetics are well-known surface reaction mechanisms which assume a single rate determining reaction on an active catalyst reaction site. The availability of these active reaction sites may be compromised by competitive adsorption of reactants, reaction intermediates and products [20]. LH kinetics have been reported by Nakagawa et al. [21] for a Ni-YSZ-CeO_2 anode, and Dicks et al. [22] derived HW kinetics for a Ni-YSZ anode.

The majority of the internal MSR kinetics reported for SOFCs is of the PL type, especially those derived on functional anodes. These models implicitly assume that the complex surface chemistry involved in the reforming reaction can be disregarded and the kinetics are described by global reaction orders for the reactants and sometimes products involved in the reaction instead. PL kinetics for SOFC cermet anodes are, among others, derived by Ahmed et al. [23], Timmerman et al. [24] and Fan et al. [25].

Some authors simplify the kinetics even further and assume that the MSR is approximately first order (FO) in methane and influences of other reactants and products can be neglected. For example, Belyaev et al. [26] reported such kinetics for a Ni-ZrO_2-CeO_2 electrode. The FO kinetics reported by Achenbach et al. [27] for a Ni-ZrO_2 substrate are to this day probably the most frequently applied reforming model in reduced order and control-oriented dynamic SOFC stack models [8,28].

Global reaction mechanisms, such as PL or FO, may capture the rate determining step in specific cases, for example if the adsorption of a single reactant is rate limiting and there is no inhibiting effect of other species on the catalyst surface. However, they may not capture the rate limiting step when the operating conditions change. This was demonstrated in previous work, where a PL rate equation was shown to predict the global reforming rates with accuracies comparable with an intrinsic HW model, but the local reaction rate predicted by the two models differed substantially [29].

Extensive multi-step reaction mechanisms, as developed by Hecht et al. [18], can fully describe the complex interdependency between surface adsorption, desorption and surface coverage by reaction intermediates. However, their parameterisation requires a substantial amount experimental data, since such models have a many degrees of freedom. Developing multi-step reforming kinetics based on data obtained on functional cell assemblies is, therefore, challenging. Instead, reforming experiments are usually conducted on substrate materials rather than complete cell assemblies [18,22,27].

Although detailed mechanistic studies are indispensable to understand the complex surface chemistry of the reforming reaction, it is difficult to use kinetics derived on different materials with deviating thicknesses, pore size distribution, particle size distribution and catalyst loading into control-oriented dynamic stack models of SOFC stacks [11]. Moreover, a large and stiff system of equations is obtained which is not convenient for application in control-oriented dynamic models [30]. In addition, MSR kinetics have been primarily investigated for porous, electrochemically inactive Ni-YSZ substrates, while ceria-based cermet anodes are increasingly used as they are reported to have a higher tolerance to carbon deposition [31].

MSR was studied on Ni-GDC anodes of functional SOFC assemblies in previous experimental work in this group, both under open and closed circuit conditions [25,30]. The methane partial pressure was shown to have a promoting effect on the reaction rate, while steam was shown to affect the reforming rate negatively. Although the hydrogen oxidation reaction increases the steam concentration as well, it consistently increased the overall reforming rate in the experiments. This may be explained by a non-monotonic dependency on the steam partial pressure, the increased driving force due to the addition of steam, a local increase of the cell temperature or so-called *non-faradaic electrochemical modification of catalytic activity (NEMCA)* [32].

In a follow-up study, kinetic models of the PL and HW type were regressed from the experimental data and implemented in a 3D CFD model of the single cell test station [29]. Both kinetic models showed good agreement with the original data derived on single cells. However, the PL kinetics predicted a relatively flat reaction rate distribution along the flow direction, while the reforming rate decreased sharply from inlet to outlet according to the HW mechanism. As a result, higher temperature gradients were predicted with the HW than the PL kinetics.

HW kinetics have been proposed for the MSR reaction, and a dependency on the steam-to-hydrogen (SH) ratio is commonly reported [12,13,22,29,30,33,34]. However, the SH ratio varies from inlet to outlet in DIR SOFCs. Steam is usually mixed with the unreformed fuel to suppress the solid carbon formation through the methane dissociation, Boudouard and reverse gas shift reactions, thus leading to a high SH

ratio at the inlet [35]. The SH then decreases as steam is consumed and hydrogen is produced by the MSR reaction, after which the SH increases again due to the hydrogen oxidation reaction. Therefore, intrinsic reforming kinetics need to capture the effect of the SH ratio correctly.

The influence of methane and steam is commonly quantified in experimental studies and accounted for in rate equations, but the effect of hydrogen is rarely reported. Therefore, most MSR models may not capture the rate limiting step due to the large SH variations in DIR SOFCs. Dicks et al. [22] studied the effect of the hydrogen partial pressure on the reforming rate experimentally, reporting an enhancing effect. However, in other studies the effect of hydrogen is commonly included on the basis of data fitting adequacy only [30,33]. Therefore, further study of the rate limiting step in the intrinsic MSR kinetics on SOFC anodes is required, taking into account the influence of the SH ratio.

Previous experimental work on DIR in Ni-GDC anodes of functional SOFC assemblies focussed on the influence of the partial pressures of methane and steam and the electrochemical reaction. The results of Fan et al. [25] demonstrated the need to derive detailed surface reaction mechanisms on functional SOFC assemblies, and HW kinetics were subsequently derived by Thattai et al. [30]. These kinetics suggest that the hydrogen partial pressure affects the DIR rate, but this hypothesis could not be confirmed as the effect of hydrogen was not studied in the experiment.

In this study, not only the influence of the partial pressures of methane and steam on the direct internal MSR are investigated, but the hydrogen partial pressure as well. Experimental methane reforming rates are derived on functional single cell SOFCs with Ni-GDC cermet anodes for various fuel gas compositions and temperatures. The conversions are then used to regress kinetic models of the FO, PL, LH and HW type for the internal MSR reaction. These kinetic models are then compared to select the most adequate reaction mechanism.

2. Experimental

2.1. Experimental setup

The reforming experiments are carried out in a single cell test setup, shown in Fig. 1, on a 10 × 10 cm electrolyte supported cell (ECS2, H.C. Starck) with a 100 μm thick YSZ electrolyte, an active area of 81 cm^2 (9 × 9 cm) and a 35 μm thick Ni-GDC (Ni-$Gd_{0.1}Ce_{0.9}O_{1.95}$) cermet anode consisting of approximately 57 wt% NiO. A 40 μm thick layer of LSM ($La_{1-x}Sr_xMnO_{3-\delta}$) functions as the cathode.

The cells are placed in a ceramic holder with fuel and air manifolding. A 0.5 mm platinum mesh serves as a current collector on both anode and cathode side. A 0.54 mm ceramic seal is placed at the anode side, and a 0.5 mm thermiculite (mica) frame seals the cathode side. Weight is added on top of the ceramic holder to compress the mica seal and ensure gas tightness of the assembly, as well as proper electrode-current collector contact.

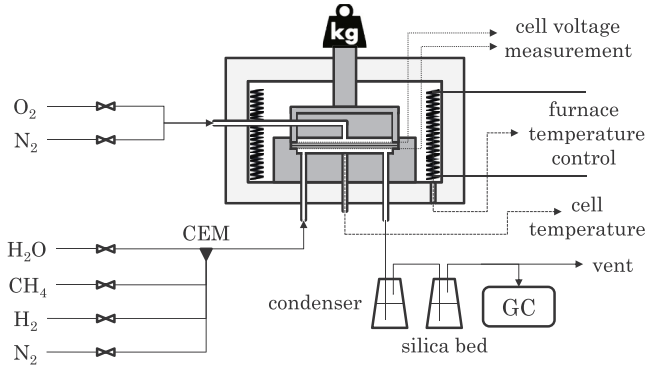

Fig. 1. Schematic overview of the experimental single cell setup.

Dry gases are supplied from gas bottles and controlled with mass flow controllers (Bronkhorst EL-FLOW). Steam is mixed with the dry gases using a controlled evaporator mixer (Bronkhorst LiQUI-FLOW and CEM). The temperature is controlled with thermocouples located in the furnace heating coils and the ceramic cell holder, close to the centre of the cell. The furnace heating power is controlled through the temperature of the heating coils and adjusted to maintain a constant temperature of the ceramic cell holder for different gas composition, assuming that the cell temperature is approximately equal.

2.2. Catalyst reduction, gas analysis and stability

The nickel catalyst is reduced by increasing the hydrogen concentration in the feed gas from 2 to 100 vol% over a period of 4 h at a temperature of 950°C. This procedure was developed and used in previous experiments on the same type of cells [25,30]. The current-voltage characteristics are then determined to verify that the cell is successfully reduced.

A gas chromatograph (Agilent 490 micro gas chromatograph) is used to analyse the dried anode outlet gas composition. The anode off-gas is passed through a water bubbling condenser to remove steam, and further dried in a silica gel bed to prevent moisture from entering the gas chromatograph. The mole fractions of hydrogen, methane, carbon monoxide and nitrogen are analysed using a Molsieve 5A column, while the concentration of carbon dioxide in the dry gas is determined with the aid of a PoraPLOT U column. An external method, calibrated using gas bottles with known compositions, is used to calculate the gas concentrations in the sampled dry anode gas.

The methane conversion in the experiment is calculated from a carbon balance assuming that methane is converted to *CO* and CO_2 only:

$$x_{CH_4} = \frac{n^{in}_{CH_4} - n^{out}_{CH_4}}{n^{in}_{CH_4}} = \frac{y_{CO} + y_{CO_2}}{y_{CO} + y_{CO_2} + y_{CH_4}}, \quad (4)$$

where y_i is the molar fraction of species *i*. It was shown in previous work that reforming on the current collector can be neglected for temperatures below 800°C, hence all reforming can be assumed to take place on the SOFC anode [30].

Fig. 2a shows an example of the dry composition obtained from gas analysis over time, compared to the dry composition calculated from the carbon balance in Equation (4), assuming that the WGS reaction is in chemical equilibrium. This result confirms the gas analysis is accurate for the compositions of interest, since the calculated nitrogen and hydrogen mole fractions match well with the values determined with gas chromatography.

Additional tests are carried out to verify the stability and reproducibility of the experimental results. Fig. 2b shows that the reforming rate stabilises within 24 h after switching from dry hydrogen to a mixture containing methane and steam. The reforming rate is found to be stable few hours after changing the experimental temperature, and within an hour after the gas composition is changed.

2.3. Reforming experiments

The conditions for the reforming experiments are chosen such that:

- The temperatures and gas compositions are relevant for SOFC operating conditions;
- The conditions differ sufficiently from each other to reveal significant dependencies;
- The effects of the methane, steam and hydrogen partial pressure and temperature can be determined independent from each other.

As such, the gas composition and temperature are varied within a relevant range, but do not represent specific SOFC operating points. The

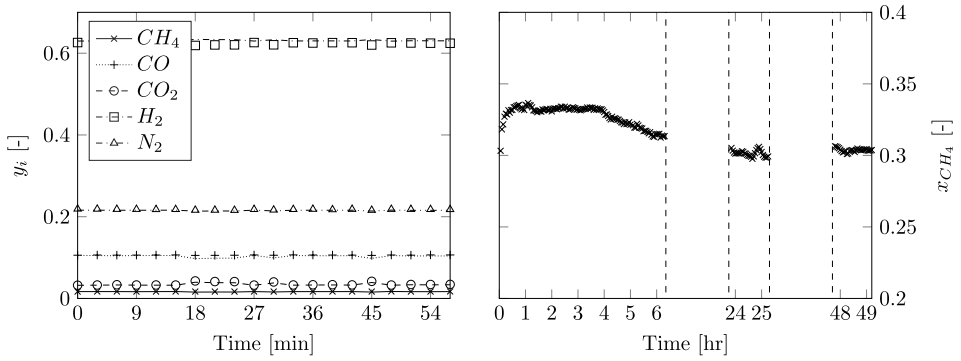

(a) Measured and calculated gas composition. (b) Stabilisation of methane conversion.

Fig. 2. Measured dry gas composition (symbols) compared to the calculated with Equation (4) (lines) (Fig. 2a) and stabilisation of the methane conversion at 700°C after switching from dry hydrogen to methane (Fig. 2b).

methane mole fraction and total flow rates are chosen such that the experimental methane conversions are always well below chemical equilibrium, to ensure that the reforming rate is limited by the kinetics of the reforming reaction. A flow of 2 Nl min^{-1} simulated air with 80 vol % nitrogen and 20 vol% oxygen is supplied at the cathode.

Various fuel compositions with methane, steam and hydrogen are supplied to the anode, and nitrogen is added to maintain a constant total volume flow rate of 2 Nl min^{-1}. The SC ratio is varied from 1.5 to 3, which is a common range used to prevent carbon deposition. The SH ratio is varied from 1 to 18, representing the varying hydrogen and steam concentrations from inlet to outlet. Table 1 provides an overview of the experimental gas compositions.

The experiments are carried out at cell temperatures of 700, 725, 750 and 775°C, as these are close to the temperature typically encountered at the entrance region of a SOFC stack. No current was drawn from the cell during the reforming experiments, although current-voltage characteristics were occasionally determined to verify that the cell was still functional.

The experiments were conducted over a consecutive period of twelve days, or about 280 h, with the cell continuously operating under internal reforming conditions. The reforming rate was stabilised for at least 2 h after changing the gas composition, and over night after changing the temperature. The SOFC performance was stable over this period as well as in the 14 days prior to the experiment, during which initial tests were conducted to determine appropriate gas compositions, flows and stabilisation times.

2.4. Carbon deposition

Solid carbon formation can deteriorate the anode by blocking pores and reactions sides. Therefore, carbon deposition should be avoided during normal SOFC operation. Carbon deposition might occur via the methane cracking, Boudouard and reverse gasification reactions:

$$CH_4 \rightleftharpoons C(s) + 2H_2 \quad (5)$$

$$2CO \rightleftharpoons C(s) + CO_2 \quad (6)$$

$$H_2 + CO \rightleftharpoons C(s) + H_2O \quad (7)$$

In addition, cerium oxide possesses improved resistance against carbon depositing due to its oxygen storage capacity. Solid carbon deposited on the catalyst suface may be removed by a reaction with lattice oxygen:

$$nC(s) + CeO_2 \rightleftharpoons nCO + CeO_{2-n} \quad (8)$$

Whether carbon deposition is thermodynamically favourable depends on the gas composition, temperature, pressure and type of carbon formed, and can be determined from equilibrium calculations. Fig. 3a indicates C-H-O compositions for which carbon formation is thermodynamically expected in a ternary diagram at a temperature of 700°C, assuming that the carbon type formed is graphite. The experimental gas compositions from Table 1 are indicated in Fig. 3a as well, revealing that the formation of this type of carbon is thermodynamically not expected.

Although graphite formation is thermodynamically not expected, it may still occur if the speed of individual carbon deposition reactions is higher than the removal reactions [36]. In addition, other types of carbon with different thermodynamic properties, such carbon nano fibres, may form on the anode. To ensure that the cell is not degraded by carbon deposition, the cell is cooled down after the experiment in inert gases (nitrogen) and analysed with scanning electron microscopy (SEM) and energy dispersive X-ray spectroscopy (EDX). The EDX analysis in Fig. 3b shows the expected peaks for nickel, cerium, and gadolinium, but not for carbon, which would be expected at 0.227 keV.

Table 1
Experimental anode inlet gas compositions and the SC and SH ratios.

Composition	y [-]				SC	SH
	CH_4	H_2O	H_2	N_2		
A	0.18	0.36	0.36	0.1	2	1
B	0.18	0.36	0.18	0.28	2	2
C	0.18	0.36	0.12	0.34	2	3
D	0.18	0.36	0.04	0.42	2	9
E	0.2	0.36	0.04	0.4	1.8	9
F	0.22	0.36	0.04	0.38	1.64	9
G	0.24	0.36	0.04	0.36	1.5	9
H	0.24	0.48	0.04	0.24	2	12
I	0.24	0.6	0.04	0.12	2.5	15
J	0.24	0.72	0.04	0	3	18

Total flow = 2 Nl min^{-1}, T = 700, 725, 750 and 775°C.

3. Kinetic model regression

The experimental methane conversions are used to parameterise different rate equations for the MSR reaction using an ideal plug flow reactor (IPFR) model, developed for this purpose. The following sections provide details on the assumption in the IPFR model, the kinetic models parameterised and the regression method employed.

3.1. Ideal plug flow reactor model

The IPFR model assumes that the reacting flow passes through a catalyst bed while it is ideally mixed in the radial direction, but axial diffusion or mixing does not take place. In that case, the reaction rate for an infinitely small reactor area is given by

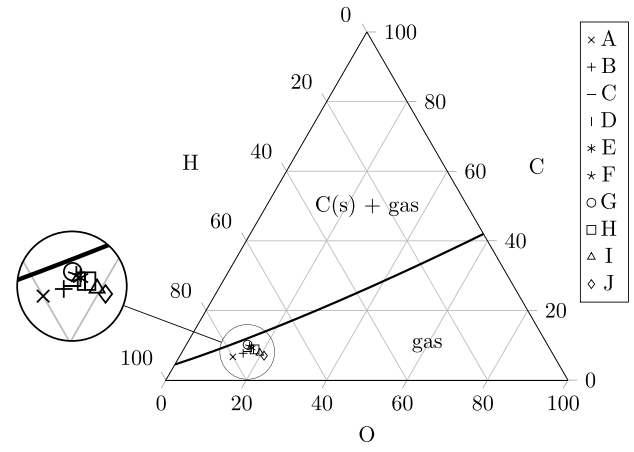

(a) Ternary diagram for a C-H-O mixture.

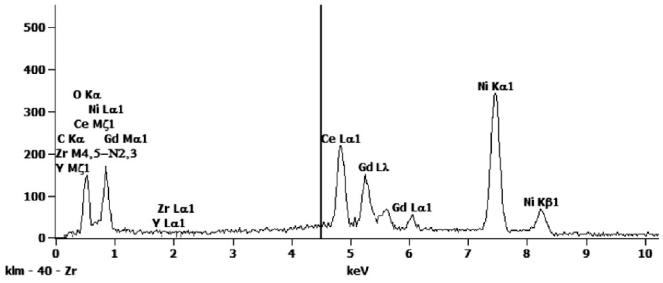

(b) EDX analysis after experiment.

Fig. 3. Ternary diagram for solid carbon formation (Fig. 3a) and the result of an EDX analysis showing no carbon peak at 0.277 keV (Fig. 3b).

$$-r_{msr} = \frac{d(n_{CH_4})}{dA} = \frac{d\left(n^{in}_{CH_4}\,(1 - x_{CH_4})\right)}{dA} = -\,n^{in}_{CH_4}\frac{d(x_{CH_4})}{dA}, \tag{9}$$

where r_{msr} is the area specific reforming rate, n_{CH_4} is the molar flow of methane and A is the active cell area. The total active cell area then follows from:

$$A = n^{in}_{CH_4}\int_0^{x^{out}_{CH_4}} \frac{dx_{CH_4}}{r_{msr}} \tag{10}$$

Since the active cell area is known, this equation can be used to regress parameters in an expression for the reaction rate r_{msr}, provided that it is a function of methane conversion x_{CH_4}. Reaction rates of gasses are generally written as a function of the partial pressures of reactants and products, as these can be assumed to be proportional to the activity of ideal gasses. Therefore, the partial pressures of the gasses are written as function of the methane conversion rate. The partial pressures in the gas mixture follow from:

$$p_{CH_4} = \psi\,(1 - x_{CH_4}) \tag{11}$$

$$p_{H_2O} = \psi\,(SC - x_{CH_4} - x_{CO}) \tag{12}$$

$$p_{H_2} = \psi\,(HC + 3x_{CH_4} + x_{CO}) \tag{13}$$

$$p_{CO} = \psi\,(x_{CH_4} - x_{CO}) \tag{14}$$

$$p_{CO_2} = \psi\,x_{CO} \tag{15}$$

Here, SC and HC are the steam- and hydrogen-to-carbon ratio respectively and x_{CO} is the fraction of carbon monoxide that is converted to carbon dioxide via the WGS reaction. The factor ψ corrects for the total experimental pressure and the increase in the molar flow due to the MSR reaction

$$\psi = p\left(\frac{\sum_i n^{in}_i}{n^{in}_{CH_4}} + 2\,x_{CH_4}\right)^{-1}, \tag{16}$$

where p is the total pressure in the experiment. The WGS reaction can be assumed to be in chemical equilibrium along the reactor, as it generally proceeds much faster than the MSR reaction [8]. The equilibrium can be calculated using the van 't Hoff relation:

$$K_{eq,wgs} = exp\left(\frac{\Delta G^0_{wgs}}{RT}\right) = \frac{p_{CO_2}\,p_{H_2}}{p_{CO}\,p_{H_2O}} \tag{17}$$

Equations (12) to (15) and (17) can be subsequently solved to obtain an expression for x_{CO} as a function of SC, HC, $K_{eq,wgs}$ and x_{CH_4}. In this way expressions are derived for the partial pressures in the reacting gas mix as a function of the experimental conditions and x_{CH_4}. The constant active cell area is now expressed as a function of the experimental conditions and the rate expression using Equation (10). Since the active cell area is known and constant, this equation is used to regress parameters in kinetic models.

3.2. Kinetic models

The objective of this study is to identify the rate determining kinetics of the MSR on Ni-GDC anodes, which may be captured by a classical surface reaction model, such as LH or HW kinetics, or a global model, for example PL or FO kinetics [30]. The PL, FO, LH and HW kinetics are described in this section.

3.2.1. Power law and first order kinetics

PL expressions provide a convenient means to describe the dependency of the rate of a chemical reaction without knowledge of the complex surface chemistry involved. Since the partial pressures of methane, steam and hydrogen were varied in the experiment, the PL equation takes the form

$$r_{msr} = k\,p^{\alpha}_{CH_4}\,p^{\beta}_{H_2O}\,p^{\gamma}_{H_2}\left(1 - \frac{Q_{msr}}{K_{msr}}\right), \tag{18}$$

where the quotient of the reaction quotient Q_{msr} and the equilibrium constant for the MSR reaction K_{msr} determines the deviation from chemical equilibrium and, hence, the driving force of the reaction:

$$\left(1 - \frac{Q_{msr}}{K_{msr}}\right) = 1 - \frac{1}{K_{msr}}\,\frac{p_{CO}\,p^3_{H_2}}{p_{CH_4}\,p_{H_2O}} = (\text{driving force}) \tag{19}$$

The values reported in literature for the reaction orders α, β and γ vary. Although the reaction order for methane is commonly reported to be around unity, reaction orders for steam vary from −2 to 2 in literature. The influence of the hydrogen partial pressure is rarely reported. An Arrhenius temperature dependency is usually assumed for the rate constant k:

$$k = k_0\,exp\left(-\frac{E_a}{RT}\right) \tag{20}$$

The FO expression is essentially similar to the PL equation, but assumes that the reaction is first order in methane and independent of the partial pressures of other reactants and products. FO kinetics have, for example, been reported by Achenbach and Riensche [27] for SOFC cermet anodes. Although FO kinetics may appear somewhat crude, the reaction orders reported with regard to methane are indeed often close to unity. In addition, parameterising a FO reaction model is relatively straightforward, as only the temperature dependent reaction constant has to be determined experimentally.

3.2.2. Langmuir-Hinshelwood kinetics

LH kinetics are commonly used to describe the surface chemistry

involved in catalysed reactions. The fractional surface coverage of reactants and products is described by Langmuir isotherms. Generally, surface reaction models take the form

$$r = \frac{(\text{kinetic factor})}{(\text{adsorption isotherm})}\,(\text{driving force}), \tag{21}$$

where the kinetic factor describes the dependency of the rate determining step on the gas species involved, the adsorption isotherm accounts for the available active reaction sites and the driving force similar as introduced in the Power-Law rate equation.

LH kinetics assume that a bimolecular reaction between two reactants adsorbed on neighbouring sites is slowest and, therefore, rate determining. Surface adsorption is described by Langmuir isotherms, leading to:

$$r_{msr} = \frac{k\, K_{CH_4}\, K_{H_2O}\, p_{CH_4}^{\alpha}\, p_{H_2O}^{\beta}}{\left(1 + K_{CH_4}\, p_{CH_4}^{\alpha} + K_{H_2O}\, p_{H_2O}^{\beta}\right)^{\gamma}} \left(1 - \frac{Q_{msr}}{K_{msr}}\right) \tag{22}$$

Here, K_i is the adsorption constant of species i. The values of α and β depend on the specific adsorption mechanism on the catalyst surface, i.e. the number of unoccupied reaction sites required for adsorption, and γ is the number of active reaction sites involved in the rate determining step. Adsorption groups in Equation (22) may be neglected if their adsorption is low. The adsorption enthalpies and entropies follow from the van 't Hoff relation. Hence, the temperature dependence of the Langmuir adsorption constants follows from:

$$K_{ad} = A_{ad}\, exp\left(-\frac{\Delta H_{ad}}{RT}\right) \tag{23}$$

Thermodynamic consistency requires that $A_{ad} > 0$ and $\Delta H_{ad} < 0$, such that the adsorption constant K_{ad} is positive and decreases with temperature.

3.2.3. Hougen-Watson kinetics

The classical LH equation was extended by Hougen and Watson for complex surface reactions. The possible rate determining step is not limited to reactions on the catalyst surface, but may originate from adsorption, formation and desorption of reactants, products and reaction intermediates. In addition, the adsorption isotherm may contain reaction intermediates and products as well.

HW kinetics have been reported both for MSR on industrial catalysts, for example be Xu et al. [12] and Hou et al. [13], and SOFC anodes by Dicks et al. [22] and Thattai et al. [30]. In these studies, rate expressions are reported of the form

$$r_{msr} = \frac{k\, p_{CH_4}\, p_{H_2O}^{\alpha} \Big/ p_{H_2}^{\beta}}{\left(1 + \cdots + K_{H_2O}\frac{p_{H_2O}}{p_{H_2}}\right)^{\gamma}} \left(1 - \frac{Q_{msr}}{K_{msr}}\right) \tag{24}$$

The adsorption of oxygen as a surface intermediate, described by the adsorption group $K_{H_2O}\frac{p_{H_2O}}{p_{H_2}}$, is reported in many studies. Values of 0–1 are reported for β, while the value of γ may be as high as 2.5. Adsorption effects from carbon monoxide and hydrogen are commonly reported as well.

3.2.4. Parameter regression

The kinetic models introduced in Section 3.2 are parameterised and evaluated using the IPFR model described in Section 3.1. The algorithm uses Equation (10), which calculates the known active area A, to parameterise different kinetic models. The regression of PL kinetics does not require an elaborate approach, as all parameters are functions of different independent variables: the reaction orders are determined by different reactant and product partial pressures, and the activation energy by the temperature dependence. LH and HW kinetics, however, contain several temperature dependent constants. Therefore, all constants are functions of the temperature and regression is aided with a more accurate initial guess. The algorithm comprises three consecutive steps to efficiently regress the non-linear set of equations:

- Minimisation of the coefficient of variation of A for each individual experimental temperature to obtain initial guesses of rate constants, reaction orders and adsorption constants for the next step;
- Minimisation of the coefficient of variation of A including the logarithmic temperature dependence of rate and adsorption constants to obtain an initial guess for the final step;
- Minimisation of $\left|1 - \mathrm{R}^2\right|$ for the entire data set. Equation (10) is solved for $x_{CH_4}^{out}$ with the known active area A for this purpose to predict overall methane reforming rates with the IPFR model for the kinetics of interest.

The Nelder-Mead simplex algorithm is employed in each subsequent minimisation step. A schematic overview of this procedure is shown in Fig. 4b.

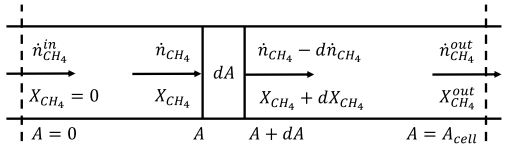

(a) IPFR reactor model.

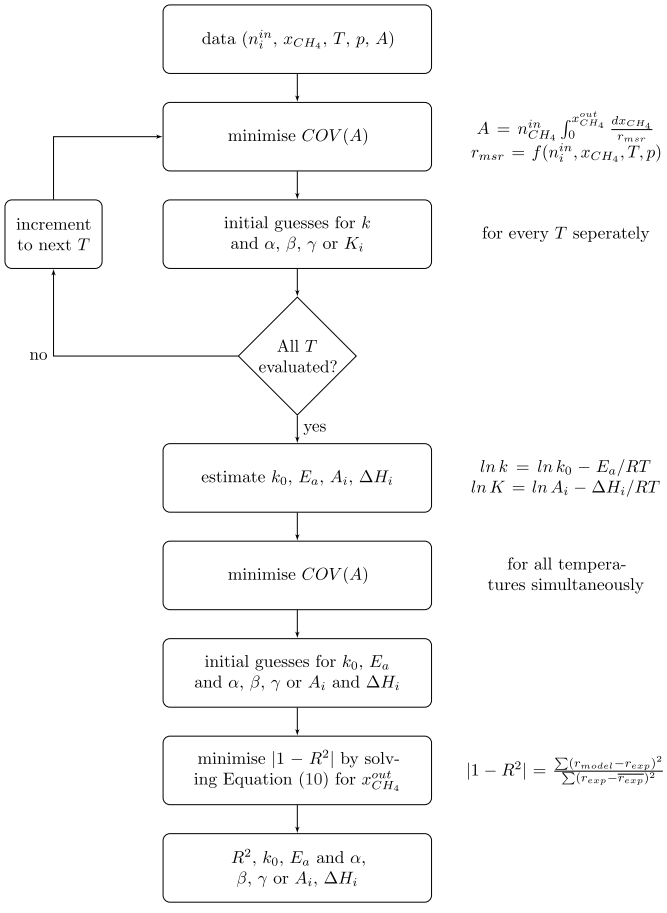

(b) Model regression flowchart.

Fig. 4. Schematic overview of the IPFR reactor model (Fig. 4a) and a flowchart of the procedure used to regress the kinetic model parameters (Fig. 4b).

3.3. Thermodynamic consistency

The Langmuir adsorption constant in Langmuir-Hinshelwood and Hougen-Watson models should be thermodynamically consistent and therefore, meet three thermodynamic rules and two guidelines [12,19,20]:

- **Rule 1**: Adsorption is an exothermic process. Therefore, the enthalpy of adsorption at the reference state should be negative: $\Delta H^0_{ad} < 0$.
- **Rule 2 & 3**: The entropy should decrease after adsorption, thus $\Delta S^0_{ad} < 0$(rule 2). Moreover, a molecule can only lose the entropy it possessed prior to adsorption (rule 3). Hence, $-\Delta S^0_{ad} < S^0_g$. Together, these rules lead to $0 < -\Delta S^0_{ad} < S^0_g$.
- **Guideline 1 & 2**: Two guidelines have been proposed to further assess the plausibility of the adsorption constants. Combined these empirical relations yield $10 \leq -\Delta S^0_{ad} \leq 12.2 - 0.0014\,\Delta H^0_{ad}$, with the units of energy in cal mol^{-1}. Converted to J mol^{-1} this gives $41.84 \leq -\Delta S^0_{ad} \leq 51.04 - 0.0014\,\Delta H^0_{ad}$.

These rules and guidelines are evaluated using the van 't Hoff equation

$$ln(K) = -\frac{\Delta G^0_{ad}}{RT} = -\frac{\Delta H^0_{ad}}{RT} + \frac{\Delta S^0_{ad}}{R}, \quad (25)$$

thus the entropy of adsorption is calculated from the adsorption constants:

$$\Delta S^0_{ad} = ln(A_{ad}) \cdot R \quad (26)$$

It is evident from Equation (25) that the value of ΔS^0_{ad} depends on the units of the pre-exponential factor A_{ad}, which is important to obtain meaningful results [19,20]. The enthalpy and entropy values should be taken at the reference state, which is atmospheric pressure for both the tabulated gas phase entropy values and constants in the empirical guidelines. Therefore, the pressure units in A_{ad}, if any, should be either taken in atm, or the gas phase entropies and empirical constants have to be converted to consistent units.

4. Results

4.1. Experiments

The experimental data obtained in the experiment is shown in Table 2 and Fig. 5. Fig. 5a shows that a higher methane partial pressure results in a higher reforming rate, which is consistent with previous findings. Fig. 5b reveals a slight decrease in the MSR rate for higher steam partial pressures, which seems to be more pronounced for lower temperatures and reforming rates. Finally, Fig. 5c shows the influence of the hydrogen partial pressure on the overall reaction rate. A slight increment in the reforming rate is apparent for higher hydrogen partial pressures is apparent.

The experimentally observed influence of the methane and steam partial pressures on the reforming rate agree with the trends reported in earlier work on Ni-GDC anodes [25,30]: A non-proportional but strong influence of the methane partial pressure and a slight but significant effect of higher steam partial pressures. A negative effect of a higher steam partial pressure on the reaction rate may be explained by competitive adsorption of steam or a related reaction intermediate on the catalyst surface, which limits available reaction sites. Such an effect has been reported in several experimental investigations [21–23,25,30,37].

Denominators in HW kinetics often contain an adsorption group consistent with dissociative adsorption of steam into gaseous hydrogen and surface-adsorbed oxygen:

$$K_{H_2O}\,\frac{p_{H_2O}}{p_{H_2}} \quad (27)$$

A positive effect of hydrogen is thus expected for conditions where steam is reported to have a negative influence, although this may be counteracted by a negative contribution of the hydrogen partial pressure in the kinetic factor, as proposed by Xu et al. [12]. In that case a strong non-monotonic dependency on the hydrogen partial pressure is expected, but no such effect is observed for the experimental SH ratios ranging from 1 to 18.

4.2. Parameter regression

Two global reaction mechanisms have been fitted to the experimental data: The first one first order in methane and, hence referred to as FO, and the second one of the PL type with reaction orders for the experimentally evaluated species, i.e. methane, steam and hydrogen respectively. In addition, various forms of the LH and HW kinetics have been evaluated. Especially the HW model enables many possible rate equations, as the rate determining kinetics may be governed by an adsorption or desorption step, and the adsorption group can include any reactant, product or reaction mechanism. However, any feasible reaction mechanism should:

- Provide a sound qualitative explanation for the experimental observations;
- Give a high quality fit with the experimental data, i.e. R^2 close to 1;
- Be thermodynamically consistent.

The majority of the evaluated possible kinetic expressions could be rejected as they did fail to satisfy at least one of the criteria listed above. Two models were selected as they performed equally well against the listed criteria: One with the classical LH formulation and the other of the HW type. Table 3 provides an overview of the equations obtained and the regressed parameters. In addition, Fig. 6 shows the overall reforming rates predicted by the models in Table 3 for different gas compositions and temperatures compared to the experimental values.

4.2.1. First order kinetics

The FO model is by far the most straightforward of the four models presented and only requires determination of a temperature dependent rate constant. Nonetheless, the FO model describes the experimental results with reasonable accuracy, although the activation energy of 190.5 kJ mol^{-1} is higher than what is commonly reported. With the exception of Belyaev et al. [26], who reported a value of 162 kJ mol^{-1} for a first order in methane reaction model, most authors report values ranging from 80 to 100 kJ mol^{-1}.

Table 2
Experimental methane conversion fraction x_{CH_4} for the evaluated gas compositions and temperatures.

T (°C)	Composition									
	A	B	C	D	E	F	G	H	I	J
700	0.304	0.304	0.305	0.296	0.272	0.267	0.260	0.256	0.252	0.248
725	0.443	0.435	0.437	0.432	0.432	0.417	0.409	0.402	0.389	0.373
750	0.627	0.629	0.625	0.623	0.617	0.610	0.602	0.599	0.597	0.591
775	0.794	0.787	0.786	0.784	0.772	0.764	0.755	0.762	0.765	0.752

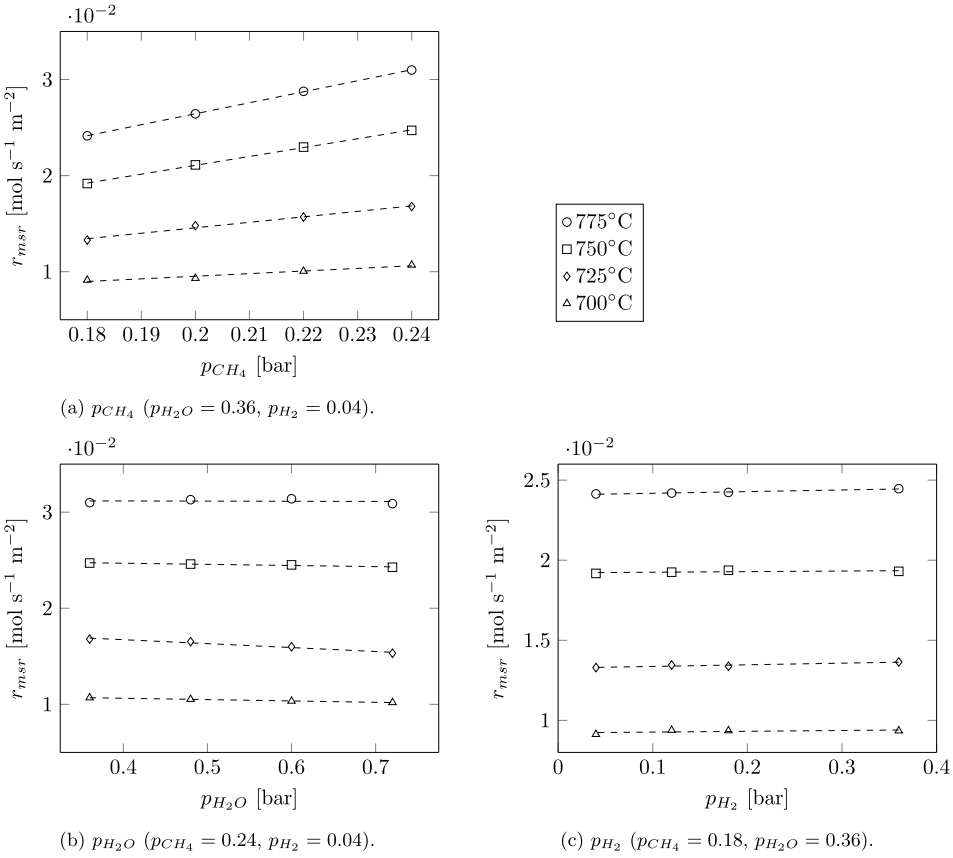

(a) p_{CH_4} ($p_{H_2O} = 0.36$, $p_{H_2} = 0.04$).

(b) p_{H_2O} ($p_{CH_4} = 0.24$, $p_{H_2} = 0.04$).

(c) p_{H_2} ($p_{CH_4} = 0.18$, $p_{H_2O} = 0.36$).

Fig. 5. Experimentally observed MSR reaction rates for the evaluated temperatures and different partial pressures of methane (Fig. 5a), steam (Fig. 5b) and hydrogen (Fig. 5c).

Table 3
Overview of the rate equations and parameters obtained through regression of the experimental data.

$$r_{msr} = k\, p_{CH_4}^{\alpha}\, p_{H_2O}^{\beta}\, p_{H_2}^{\gamma} \left(1 - \frac{Q_{msr}}{K_{msr}}\right)$$

Parameter	α [-]	β [-]	γ [-]	k_0 [mol s^{-1} m^{-2} bar$^{-\alpha-\beta-\gamma}$]	E_a [kJ mol^{-1}]	R^2
FO	1	-	-	9.472e8	190.5	0.9930
PL	0.8954	−0.0619	0.0693	9.799e7	173.1	0.9965

$$r_{msr} = \frac{k\, K_{CH_4}\, K_{H_2O}\, p_{CH_4}\, \sqrt{p_{H_2O}}}{(1 + K_{CH_4}\, p_{CH_4} + K_{H_2O}\, \sqrt{p_{H_2O}})^2} \left(1 - \frac{Q_{msr}}{K_{msr}}\right)$$

Parameter	A_{CH_4} [bar^{-1}]	ΔH_{CH_4} [kJ mol^{-1}]	A_{H_2O} [bar$^{-0.5}$]	ΔH_{H_2O} [kJ mol^{-1}]	k_0 [mol s^{-1} m^{-2}]	E_a [kJ mol^{-1}]	R^2
LH	4.2e-3	−54.76	1.9e-3	−62.17	1.467e10	207.6	0.9980

$$r_{msr} = \frac{k\, p_{CH_4}}{\left(1 + K_{CH_4}\, p_{CH_4} + K_{H_2O}\, \frac{p_{H_2O}}{p_{H_2}}\right)^2} \left(1 - \frac{Q_{msr}}{K_{msr}}\right)$$

Parameter	A_{CH_4} [bar^{-1}]	ΔH_{CH_4} [kJ mol^{-1}]	A_{H_2O} [-]	ΔH_{H_2O} [kJ mol^{-1}]	k_0 [mol s^{-1} m^{-2} bar^{-1}]	E_a [kJ mol^{-1}]	R^2
HW	2.8e-3	−48.33	6.78e-5	−45.45	2.787e7	158.5	0.9981

It is evident from Fig. 6 that the FO model predicts the influences of the methane partial pressure with reasonable accuracy, although the effect of methane seems to be overestimated for lower temperatures. As expected, the FO model does not predict a change in the overall reforming rate for higher hydrogen and steam partial pressures. Especially for high steam partial pressures and low temperatures this results in an overestimation of the reforming rate.

4.2.2. Power law kinetics

The PL model has three degrees of freedom more than the FO model, with reaction orders for methane, steam and hydrogen fitted to the experimental data. Therefore, the PL model describes the rate increasing and decreasing effects of the hydrogen and steam partial pressures respectively and the fit to the experimental data is improved. With 173.1 kJ mol^{-1} the activation energy is lower than for the FO model, but still higher than commonly reported.

The prediction of the reforming rates is particularly improved for higher steam partial pressures, since the decreasing effect of steam is now described correctly. In addition, the influence of the methane partial pressure is captured more accurately. Despite a slightly positive reaction order γ, an increase in the hydrogen partial pressure does not seem to result in a substantial increase in the reforming rate.

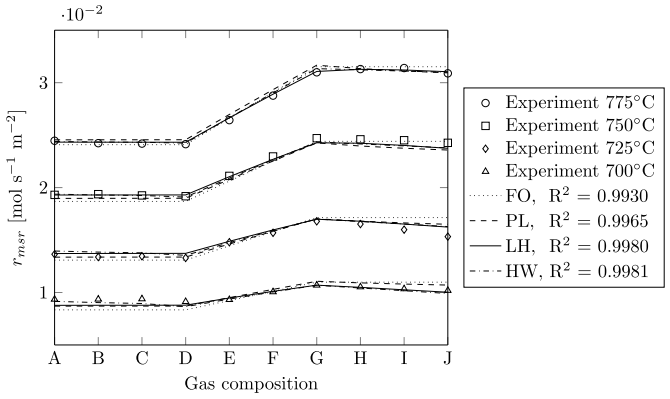

Fig. 6. Experimentally observed overall MSR rates and rates predicted in the IPFR model with the parameterised rate equations.

4.2.3. Langmuir-Hinshelwood kinetics

The LH model assumes a rate determining reaction between associatively adsorbed methane and dissociatively adsorbed steam on a single site. This mechanism is in good agreement with a methane reaction order somewhat below one in the PL model, due to competitive adsorption of methane at lower temperatures. In addition, the adsorption of steam seems in good agreement with the a decrease in the reaction rate for higher steam partial pressures, which is more pronounced at lower temperatures.

The Langmuir adsorption constants in both the LH and HW kinetics must obey the laws of thermodynamics, as discussed in Section 3.3. Table 4 shows the enthalpy and entropy of the fitted Langmuir adsorption constants for methane and steam in the LH and HW model. Table 4 shows that the enthalpies for both methane and steam are negative for the LH model, and both adsorption entropies satisfy the thermodynamic laws and guidelines as well. Therefore, the proposed LH mechanism is thermodynamically consistent.

Fig. 6 shows that the effects of the methane and steam partial pressures on the overall reforming rate are correctly captured. The LH kinetics account for the temperature dependency of the reaction site inhibiting associative adsorption of methane and dissociative adsorption of steam. Therefore, the *apparent* reaction orders for methane and steam may change with temperature, which clearly improves the agreement with the experimental data compared to the FO and PL kinetics. However, the LH kinetics do not account for influences of the hydrogen partial pressure.

4.2.4. Hougen-Watson kinetics

The kinetic factor in the HW model is first order in methane, which indicates that associative methane adsorption on the catalyst could be the rate determining step. Kinetic factors based on surface reaction or desorption controlled rate limiting step did not result in satisfactory fitting. Table 4 shows that the adsorption constants in the HW model are thermodynamically consistent. While the adsorption step in the LH model assumes dissociation into hydrogen and hydroxyl atoms

$$K_{H_2O}\, p_{H_2O}\, \theta_s^2 = \theta_{OH}\, \theta_H, \tag{28}$$

with θ_i the surface coverage of species i and s indicating an unoccupied reaction site, the HW assumes dissociation into gaseous hydrogen and surface-adsorbed oxygen, yielding:

$$K_{H_2O}\, p_{H_2O}\, \theta_s = p_{H_2}\, \theta_O \tag{29}$$

As a result, the surface coverage of oxygen will decrease for higher hydrogen partial pressures. Therefore, the dissociative adsorption group in the HW model depends on the steam-to-hydrogen ratio and not on the absolute steam partial pressure, and as such predicts an increased reforming rate for higher hydrogen partial pressures. This is in agreement with the reaction orders for steam and hydrogen in the PL model, being of equal magnitude and opposite sign.

Table 4 shows that the proposed HW mechanism is thermodynamically consistent, as the enthalpies for both methane and steam are negative and both adsorption entropies satisfy the thermodynamic laws and guidelines. Overall, the predictions of the reforming rate in Fig. 6 by the HW model are comparable to the LH kinetics. The HW kinetics account for a slight positive effect of the hydrogen partial pressure on the reforming rate, but the deviation from the LH kinetics is only visible for the lowest temperatures. As a result, the R^2 value is only marginally improved.

5. Discussion

5.1. Model comparison

Fig. 7 shows the spatial distribution of the MSR rate r_{msr} calculated with the plug flow reactor model for the different kinetic models, the four different experimental temperatures and gas composition D, the gas composition with average SC and SH ratios and minimal methane, steam and hydrogen partial pressures. All models resemble first order in methane behaviour for the highest temperatures and only deviate at the entrance region. This suggests that the MSR kinetics may be assumed to be first order in methane at temperatures $\geq$750°C. However, at lower temperatures the difference between FO and other kinetic models increases as adsorption effects become more important.

Fig. 8 shows the reforming rates predicted with the different kinetic models at 725°C and four different gas compositions: A, with the lowest SH ratio, D, with average SH and SC ratio, G, with the lowest SC ratio and J with both the highest SC and SH ratio. The kinetic models predict similar spatial distributions for gas composition A, but the predictions start to deviate as either the SH or SC ratio changes. The SH ratio affects the PL and HW kinetics in particular, while the SC ratio is important for the LH model. As a result, the predictions vary substantially for composition J, which has both the highest SH and SC ratio.

Both the FO and LH predict a monotonically decreasing MSR rate along the cell length, but the rate is initially lower according to the LH kinetics and decreases less towards the outlet. FO kinetics seem to over predict MSR at the entrance of the cell and under predict the rate at the outlet of the cell for most conditions. Both the PL and HW kinetics include an effect of the hydrogen partial pressure, which results in non-monotonic behaviour of the reaction rate: The MSR initially increases due to a promoting effect of the hydrogen partial pressure, and eventually decreases again. This is particularly the case for the HW kinetics at low temperatures and high SH ratios.

Table 4
Values of the adsorption enthalpies and entropies at reference state for methane and steam in the LH and HW kinetics, and evaluation of their thermodynamic consistency.

Model	Species	ΔH^0_{ad} [kJ mol^{-1}]	ΔS^0_{ad} [J mol^{-1} K^{-1}]	$0 < -\Delta S^0_{ad} < S^0_g$	$41.84 \leq -\Delta S^0_{ad} \leq 51.04 - 0.0014\, \Delta H^0_{ad}$
LH	CH_4	−62.17	−52.09	$0 < 52.09 < 188.8$	$41.84 \leq 52.09 \leq 138.1$
	H_2O	−62.17	−45.5	$0 < 45.5 < 186.1$	$41.84 \leq 45.5 \leq 127.7$
HW	CH_4	−48.33	−48.87	$0 < 48.33 < 188.8$	$41.84 \leq 48.33 \leq 118.7$
	H_2O	−45.45	−79.81	$0 < 79.81 < 186.1$	$41.84 \leq 79.81 \leq 114.7$

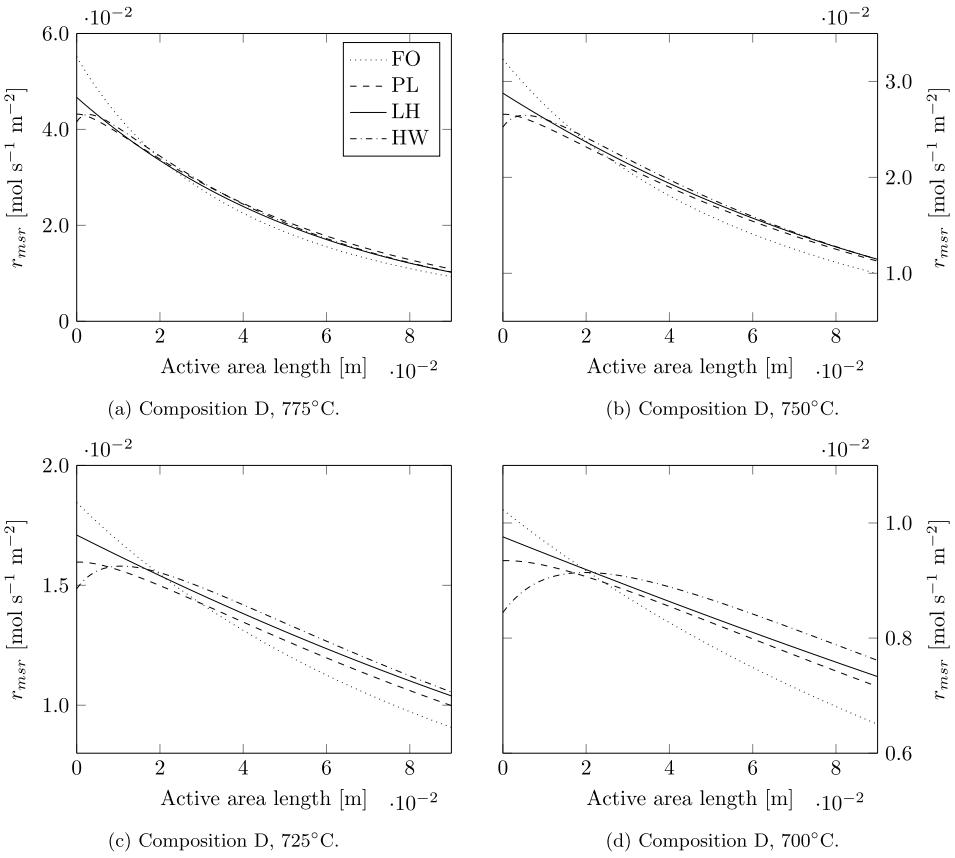

(a) Composition D, 775°C. (b) Composition D, 750°C.

(c) Composition D, 725°C. (d) Composition D, 700°C.

Fig. 7. Local MSR rate from single cell inlet to outlet predicted with the four different kinetic models and the IPFR model for four different temperatures and gas composition D.

5.2. Model selection

Global reaction kinetics can be derived from MSR data collected on complete cell assemblies with relative ease. However, they can only accurately calculate the local reforming rates and resulting thermal stresses if they capture the rate determining step. Both the FO and PL model seem to over predict the MSR reaction rate for low temperatures and high steam partial pressures. Surface reaction mechanisms, such as LH or HW kinetics, yield a single rate equation with a limited number of model parameters, while they are intrinsically valid if the rate determining step is constant for the conditions of interest.

Both the LH and HW reaction mechanism show good agreement with the experimentally observed overall MSR rates, but there are reasons to argue that the LH model is more sound than the HW mechanism. First of all, HW models can take many forms while the LH model is much more restricted. As such, there may always be a HW extension of a LH model which yields a better fit to the experimental data. However, the HW fit is not significantly better than the LH model, improving the R^2 value from 0.998 to 0.9981. The simplest model that provides a sound explanation for the experimental data is usually preferred.

Secondly, Fig. 5c shows that the effect of hydrogen is modest, even though the hydrogen molar fraction was varied from 0.04 to 0.36. It cannot be ruled out that this effect originates from measurement inaccuracies or side effects. Ceria can catalyse the MSR reaction as well, and the hydrogen partial pressure will affect the oxidation state of GDC and may, therefore, enhance the catalytic activity [38]. In addition, the thermal conductivity of hydrogen is higher than nitrogen, and replacing nitrogen with hydrogen may enhance heat transfer towards the endothermic reaction sites, increasing the local temperature.

Finally, methane adsorption is assumed to be the rate determining step in the HW model, but is included in the denominator as well. Effectively, this means that the rate limiting methane adsorption is inhibited by methane adsorbed on active sites for methane adsorption, which is physically unlikely. Although HW expressions without the methane adsorption group have been parameterised as well, these either yielded lower R^2 values than the LH model or were found to be thermodynamically inconsistent.

For all reasons listed above, the LH model is selected as the most likely reaction mechanism on the investigated Ni-GDC anode. Since the model is based on an intrinsic surface reaction mechanism, it may be applied for conditions close to the experimental range with some confidence. Moreover, it is expected to give an accurate spatial distribution of the internal reforming rate from inlet to outlet to predict temperature gradients in SOFC stacks.

5.3. Final considerations

Fan et al. [25] and Thattai et al. [30] reported MSR kinetics derived from experimental reforming data obtained on the same Ni-GDC anode cells. The strong but non-proportional dependence on the methane partial pressure and slight negative effect of the steam partial pressures were found in those studies as well. Although the activation energies were somewhat lower, the rate constants found for the three different data sets are within the same range, which gives confidence in the repeatability and applicability of the kinetics proposed in this study.

The HW kinetics proposed in previous work suggest that the hydrogen partial pressure may affect the MSR reaction rate [30]. This effect of hydrogen was based on kinetic models reported in literature and fitting adequacy, as it could explain the promoting effect of the electrochemical reaction. The influence of the hydrogen partial pressure on DIR was studied experimentally in this work. However, no evidence of a significant effect was found, hence it is unlikely that the

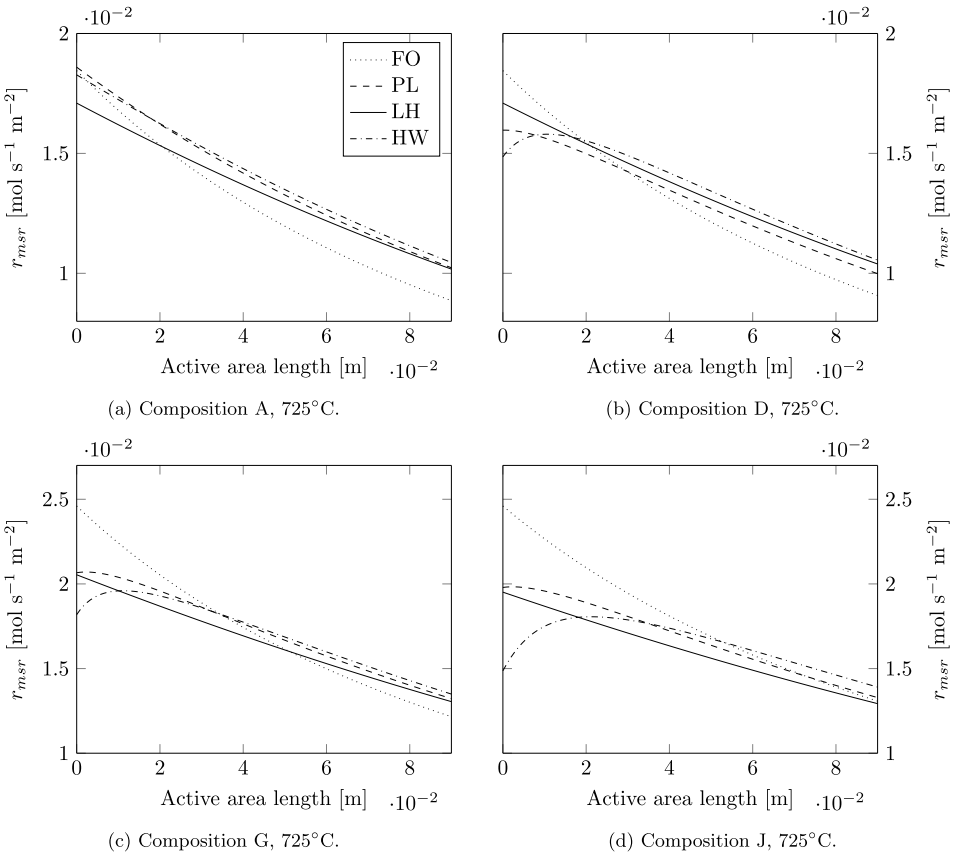

(a) Composition A, 725°C. (b) Composition D, 725°C.

(c) Composition G, 725°C. (d) Composition J, 725°C.

Fig. 8. Local MSR rate from single cell inlet to outlet predicted with the four different kinetic models and the IPFR model for four different gas compositions at 725°C.

electrochemical reaction promotes the DIR rate by decreasing the hydrogen partial pressure.

Detailed information of temperatures and gas compositions along the cell would allow to discriminate between different kinetic models based on the temperature profile along the cell, since the distribution of the reaction rate predicted with the models is distinctively different (Figs. 7 and 8). However, the current experimental setup does not allow to determine temperatures and gas compositions in situ, e.g. along the cell length. Therefore, work is commencing on a modification that should enable us to determine the temperature profile with non-intrusive techniques.

Although typical electrochemical degradation rates of commercial SOFCs are <1%/1000 h [39], the DIR experiments carried out in this work may induce cumulative damage to the cell. The reduction in the catalytic activity towards the DIR reaction is not necessarily proportional to electrochemical degradation, since the degradation mechanism may be different. However, it cannot be ruled out that the reforming measurements are to some extend affected by enhanced cell degradation.

The SOFC performed stable during the experimental campaign, and no evidence for carbon deposition was found in an ex-situ analysis after the experiment. In addition, the open circuit voltage, tracked during the reforming experiments to monitor the stability of the cell, did not reveal enhanced degradation rates. Nonetheless, it is advised to quantify the both electrochemical degradation and the decrease in the MSR rate due to cell degradation in future experiments, both to ascertain that degradation did not affect the kinetic model fits and validate the degradation rates reported in literature.

6. Conclusions

An experimental investigation into the individual influences of the methane, steam and hydrogen partial pressures on the direct internal MSR reaction on a functional Ni-GDC cermet anode of a single electrolyte supported SOFC was presented. A strong but non-proportional dependence of the MSR rate on the methane partial pressure and a slight negative dependence on the steam partial pressure was found. This is in good agreement with previously reported data for similar single cells. Despite the evaluation of a wide range of hydrogen partial pressures no significant effect on the MSR was observed.

An IPFR model was used to regress kinetic parameter for rate equations of the PL, FO, LH and HW type. It was shown that all four kinetic models can predict the experimental overall reforming rates with reasonable accuracies. However, the global PL and FO kinetics were found to over predict the reforming kinetics for lower temperatures and higher steam partial pressures. Intrinsic LH and HW kinetics performed equally well, but a LH mechanism for associative adsorption of methane and dissociative adsorption of steam

$$r_{msr} = \frac{k\, K_{CH_4}\, K_{H_2O}\, p_{CH_4}\, \sqrt{p_{H_2O}}}{\left(1 + K_{CH_4}\, p_{CH_4} + K_{H_2O}\, \sqrt{p_{H_2O}}\right)^2} \left(1 - \frac{Q_{msr}}{K_{msr}}\right), \tag{30}$$

was selected because it showed good statistical agreement with the experimental data, provided a simple and physically sound explanation and was thermodynamically consistent. The kinetic model was shown to be in good agreement with results obtained in previous experiments on similar single cells with Ni-GDC anodes.

In future work, the LH kinetics will be implemented in a control-oriented 1D dynamic stack model of a DIR SOFC with Ni-GDC anodes, developed in previous work. The stack model can calculate the spatial distributions of species and temperature in the stack for different system configurations and operating conditions and predict the electrochemical performance as well as potentially deteriorating temperature gradients. The model can then be used to improve system designs and control

strategies.

Acknowledgements

This research is supported by the project *"GasDrive: Minimizing emissions and energy losses at sea with LNG combined prime movers, underwater exhausts and nano hull materials"* (project 14504) of the Netherlands Organisation for Scientific Research (NWO), domain Applied and Engineering Sciences (TTW).

References

[1] H.J. Schellnhuber, S. Rahmstorf, R. Winkelmann, Why the right climate target was agreed in paris, Nat. Clim. Chang. 6 (7) (2016) 649–653.
[2] L. Kitzing, C. Mitchell, P.E. Morthorst, Renewable energy policies in europe: converging or diverging? Energy Policy 51 (2012) 192–201.
[3] S.H. Jensen, P.H. Larsen, M. Mogensen, Hydrogen and synthetic fuel production from renewable energy sources, Int. J. Hydrogen Energy 32 (15) (2007) 3253–3257.
[4] A.B. Stambouli, E. Traversa, Fuel cells, an alternative to standard sources of energy, Renew. Sustain. Energy Rev. 6 (3) (2002) 295–304.
[5] L. van Biert, M. Godjevac, K. Visser, P. Aravind, A review of fuel cell systems for maritime applications, J. Power Sources 327 (2016) 345–364.
[6] N. Laosiripojana, S. Assabumrungrat, Catalytic steam reforming of methane, methanol, and ethanol over Ni/YSZ: the possible use of these fuels in internal reforming SOFC, J. Power Sources 163 (2) (2007) 943–951.
[7] V.M. Janardhanan, V. Heuveline, O. Deutschmann, Performance analysis of a SOFC under direct internal reforming conditions, J. Power Sources 172 (1) (2007) 296–307.
[8] P. Aguiar, C. Adjiman, N.P. Brandon, Anode-supported intermediate temperature direct internal reforming solid oxide fuel cell. i: model-based steady-state performance, J. Power Sources 138 (1) (2004) 120–136.
[9] M. Powell, K. Meinhardt, V. Sprenkle, L. Chick, G. McVay, Demonstration of a highly efficient solid oxide fuel cell power system using adiabatic steam reforming and anode gas recirculation, J. Power Sources 205 (2012) 377–384.
[10] J.-M. Klein, Y. Bultel, S. Georges, M. Pons, Modeling of a sofc fuelled by methane: from direct internal reforming to gradual internal reforming, Chem. Eng. Sci. 62 (6) (2007) 1636–1649.
[11] L. van Biert, M. Godjevac, K. Visser, P. Aravind, Dynamic modelling of a direct internal reforming solid oxide fuel cell stack based on single cell experiments, Appl. Energy 250 (2019) 976–990.
[12] J. Xu, G.F. Froment, Methane steam reforming, methanation and water-gas shift: I. intrinsic kinetics, AIChE J. 35 (1) (1989) 88–96.
[13] K. Hou, R. Hughes, The kinetics of methane steam reforming over a ni/α-al2o catalyst, Chem. Eng. J. 82 (1–3) (2001) 311–328.
[14] P. Nehter, B. Wildrath, A. Bauschulte, K. Leites, Diesel based sofc demonstrator for maritime applications, ECS Trans. 78 (1) (2017) 171–180.
[15] J. Rechberger, R. Schauperl, J.B. Hansen, P.K. Larsen, Development of a methanol sofc apu demonstration system, ECS Trans. 25 (2) (2009) 1085–1092.
[16] D. Mogensen, J.-D. Grunwaldt, P.V. Hendriksen, K. Dam-Johansen, J. Nielsen, Internal steam reforming in solid oxide fuel cells: status and opportunities of kinetic studies and their impact on modelling, J. Power Sources 196 (1) (2011) 25–38.
[17] M. Andersson, J. Yuan, B. Sundén, Sofc modeling considering electrochemical reactions at the active three phase boundaries, Int. J. Heat Mass Transf. 55 (4) (2012) 773–788.
[18] E.S. Hecht, G.K. Gupta, H. Zhu, A.M. Dean, R.J. Kee, L. Maier, O. Deutschmann, "Methane reforming kinetics within a ni–ysz sofc anode support, Appl. Catal. Gen. 295 (1) (2005) 40–51.
[19] G.F. Froment, K.B. Bischoff, J. De Wilde, Chemical Reactor Analysis and Design, vol. 2, Wiley, New York, 1990.
[20] M.A. Vannice, W.H. Joyce, Kinetics of Catalytic Reactions, vol. 134, Springer, 2005.
[21] N. Nakagawa, H. Sagara, K. Kato, "Catalytic activity of ni–ysz–ceo2 anode for the steam reforming of methane in a direct internal-reforming solid oxide fuel cell, J. Power Sources 92 (1–2) (2001) 88–94.
[22] A. Dicks, K. Pointon, A. Siddle, Intrinsic reaction kinetics of methane steam reforming on a nickel/zirconia anode, J. Power Sources 86 (1–2) (2000) 523–530.
[23] K. Ahmed, K. Foger, Kinetics of internal steam reforming of methane on ni/ysz-based anodes for solid oxide fuel cells, Catal. Today 63 (2–4) (2000) 479–487.
[24] H. Timmermann, D. Fouquet, A. Weber, E. Ivers-Tiffée, U. Hennings, R. Reimert, Internal reforming of methane at ni/ysz and ni/cgo sofc cermet anodes, Fuel Cells 6 (3–4) (2006) 307–313.
[25] L. Fan, L. van Biert, A.T. Thattai, A. Verkooijen, P. Aravind, Study of methane steam reforming kinetics in operating solid oxide fuel cells: influence of current density, Int. J. Hydrogen Energy 40 (15) (2015) 5150–5159.
[26] V. Belyaev, T. Politova, O. Mar'ina, V. Sobyanin, Internal steam reforming of methane over ni-based electrode in solid oxide fuel cells, Appl. Catal. Gen. 133 (1) (1995) 47–57.
[27] E. Achenbach, E. Riensche, Methane/steam reforming kinetics for solid oxide fuel cells, J. Power Sources 52 (2) (1994) 283–288.
[28] H. Xi, J. Sun, A low-order dynamic model for planar solid oxide fuel cells using online iterative computation, J. Fuel Cell Sci. Technol. 5 (4) (2008), 041015.
[29] L. van Biert, A.T. Tattai, P.V. Aravind, Predicting msr rates in sofcs using experimental data and cfd methods, ECS Trans. 78 (1) (2017) 2823–2834.
[30] A.T. Thattai, L. van Biert, P. Aravind, On direct internal methane steam reforming kinetics in operating solid oxide fuel cells with nickel-ceria anodes, J. Power Sources 370 (2017) 71–86.
[31] W. Wang, S.P. Jiang, A.I.Y. Tok, L. Luo, Gdc-impregnated ni anodes for direct utilization of methane in solid oxide fuel cells, J. Power Sources 159 (1) (2006) 68–72.
[32] V. Belyaev, T. Politova, V. Sobyanin, Effect of non-faradaic electrochemical modification of catalytic activity, Solid State Ion. 136 (2000) 721–725.
[33] S. Bebelis, A. Zeritis, C. Tiropani, S.G. Neophytides, Intrinsic kinetics of the internal steam reforming of ch4 over a ni- ysz- cermet catalyst- electrode, Ind. Eng. Chem. Res. 39 (12) (2000) 4920–4927.
[34] N. Bodrov, L. Apel'baum, M. Temkin, Kinetics of the reaction of methane with water vapor on a nickel surface, Kinet. Catal. 5 (1964) 614.
[35] L. van Biert, T. Woudstra, M. Godjevac, K. Visser, P. Aravind, A thermodynamic comparison of solid oxide fuel cell-combined cycles, J. Power Sources 397 (2018) 382–396.
[36] G.J. Offer, J. Mermelstein, E. Brightman, N.P. Brandon, Thermodynamics and kinetics of the interaction of carbon and sulfur with solid oxide fuel cell anodes, J. Am. Ceram. Soc. 92 (4) (2009) 763–780.
[37] A.L. Lee, R. Zabransky, W. Huber, Internal reforming development for solid oxide fuel cells, Ind. Eng. Chem. Res. 29 (5) (1990) 766–773.
[38] E. Ramırez-Cabrera, A. Atkinson, D. Chadwick, Catalytic steam reforming of methane over ce0. 9gd0. 1o2- x, Appl. Catal. B Environ. 47 (2) (2004) 127–131.
[39] L. Blum, U. Packbier, I. Vinke, L. De Haart, Long-term testing of sofc stacks at forschungszentrum jülich, Fuel Cells 13 (4) (2013) 646–653.